Environmental Pollution 268 (2021) 115867

Contents lists available at ScienceDirect

Environmental Pollution

journal homepage: www.elsevier.com/locate/envpol

Litterfall mercury reduction on a subtropical evergreen broadleaf forest floor revealed by multi-element isotopes☆

Zhiyun Lu [a, c], Wei Yuan [b], Kang Luo [a, c], Xun Wang [d, *]

[a] Key Laboratory of Tropical Forest Ecology, Xishuangbanna Tropical Botanical Garden, Chinese Academy of Sciences, Mengla, Xishuangbanna, Yunnan, 666303, China
[b] State Key Laboratory of Environmental Geochemistry, Institute of Geochemistry, Chinese Academy of Sciences, Guiyang, 550081, China
[c] Ailaoshan Station for Subtropical Forest Ecosystem Studies, Chinese Academy of Sciences, Jingdong, Yunnan, 676200, China
[d] College of Resources and Environment, Southwest University, Chongqing, 400715, China

ARTICLE INFO

Article history:
Received 24 August 2020
Received in revised form
12 October 2020
Accepted 13 October 2020
Available online 27 October 2020

Keywords:
Stable mercury isotopes
Mercury reduction
Litterfall mercury
Carbon and nitrogen isotopes
Mercury sequestration

ABSTRACT

Litterfall mercury (Hg) deposition is the dominant source of soil Hg in forests. Identifying reduction processes and tracking the fate of legacy Hg on forest floor are challenging tasks. Interplays between isotopes of carbon (C) and nitrogen (N) may shed some lights on Hg biogeochemical processes because their biogeochemical cycling closely links with organic matters. Isotope measurements at the evergreen broadleaf forest floor at Mt. Ailao (Mountain Ailao) display that δ^{202}Hg and Δ^{199}Hg both significantly correlate with δ^{13}C and δ^{15}N in soil profiles. Data analysis results show that microbial reduction is the dominant process for the distinct δ^{202}Hg shift (up to ~1.0‰) between Oi and 0−10 cm surface mineral soil, and dark abiotic organic matter reduction is the main cause for the Δ^{199}Hg shift (~-0.18‰). Higher N in foliage leads to greater Hg concentration, and Hg^0 re-emission via microbial reduction on forest floor is likely linked to N release and immobilization on forest floor. We thus suggest that the enhanced N deposition in global forest ecosystems can potentially influence Hg uptake by vegetation and litter Hg sequestration on forest floor.

Author contribution

Zhiyun Lu: Investigation, Resources, Conceptualization, Formal analysis, Writing original draft. Wei Yuan: Investigation, Resources, Methodology, and Data curation. Kang Luo: Investigation, Resources, and Data curation. Xun Wang: Conceptualization, Formal analysis, Methodology, Visualization, Data curation, Writing original draft, review and editing, and Funding acquisition.

1. Introduction

Mercury (Hg) is a highly toxic persistent pollutant that poses a threat to health of human and ecosystems and has been as one of most concerned pollutants by UN Environment. The distinctly elevated anthropogenic Hg emissions during the past ~150 years have caused the current atmospheric Hg deposition being several times to one order of magnitude greater than the deposition rates during the preindustrial period (UN-Environment, 2019). Forest ecosystems play an important role in global Hg biogeochemical cycling, and serve as important receptors of atmospheric Hg and as sources of Hg to aquatic systems in remote regions (Lindberg et al., 2007; Pokharel and Obrist, 2011). Atmospheric Hg deposition in forest ecosystems comes from Hg^{2+} deposition via precipitation or throughfall, and Hg^0 uptake by vegetation and soil (Lindberg et al., 2007; Zhang et al., 2016b). Our knowledge on the Hg biogeochemical cycle in forests has been largely improved through investigating Hg isotopic compositions in each forest compartment.

Mercury mass-dependent fractionation (MDF, reported as δ^{202}Hg) and mass-independent fractionation (MIF, reported as Δ^{199}Hg, Δ^{200}Hg and Δ^{201}Hg) have been employed to determine the specific sources for Hg accumulation on forest floor and identify processes responsible for the Hg fate in forest ecosystems (Jiskra et al., 2015; Wang et al., 2017, 2020a, 2020b; Zhang et al., 2013; Zheng et al., 2016). Deposition sources such as those from precipitation Hg and vegetation uptake Hg show distinctly different Hg isotopic compositions, especially in their MIF signatures that precipitation Hg with positive Δ^{199}Hg, Δ^{200}Hg and Δ^{201}Hg values,

☆ This paper has been recommended for acceptance by Markus Hauck.
* Corresponding author.
E-mail address: xunwang@swu.edu.cn (X. Wang).

https://doi.org/10.1016/j.envpol.2020.115867
0269-7491/

while vegetation uptake Hg with negative Δ^{199}Hg and Δ^{201}Hg, and near 0 Δ^{200}Hg values (Blum et al., 2014; Chen et al., 2012; Demers et al., 2013; Wang et al., 2017). The process of Hg photo-reduction is associated with the magnetic isotope effect (MIE, Δ^{199}Hg:Δ^{201}Hg ~ 1) (Blum et al., 2014; Sonke, 2011), dark abiotic reduction by organic matter exhibits MIF caused by nuclear volume effect (NVE, Δ^{199}Hg:Δ^{201}Hg ~ 1.6)(Zheng and Hintelmann, 2010b), and only MDF is observed during microbial reduction (Kritee et al., 2007, 2008). Using the Hg isotopic signatures, earlier studies have identified the vegetation uptake Hg as the main source for Hg accumulation on forest floor, and microbial reduction and organic matters induced dark reduction can contribute the Hg MDF and MIF shifts during the sequestration processes of deposited Hg on forest floor (Jiskra et al., 2015; Wang et al., 2017, 2019b, 2020b; Yuan et al., 2020; Zheng et al., 2016).

Despite substantial efforts in quantifying atmospheric Hg deposition and pool sizes in forest ecosystems (Grigal, 2002; Obrist et al., 2018; Wang et al., 2016a, 2019b), identifying reduction processes and tracking the fate of legacy Hg on forest floor have proved to be more challenging (Demers et al., 2013; Obrist et al., 2018). Specifically, there is a lack of understanding on the post-depositional processes of litterfall Hg in regards to Hg re-emission from forest floor (Agnan et al., 2016; Gustin et al., 2008; Wang et al., 2020b; Zhang et al., 2017). Global metal-analysis suggested that the largest uncertainties of Hg^0 flux in terrestrial ecosystems stem from forests (−513 to 1353 Mg yr^{-1}) due to different landscapes and surface properties as well as methodological limitations (Agnan et al., 2016; Zhu et al., 2016). Quantifying influences of Hg^0 direct deposition to soil on Hg pool dynamics, specifically on Hg isotope shifts is still with significant uncertainties (Demers et al., 2013; Zheng et al., 2016). Though soils are by far the largest terrestrial carbon reservoir in terrestrial ecosystems (Whitehead, 2011), Hg dark abiotic reduction by natural organic matter (NOM), which is greatly highlighted in anoxic sediments and water (Gu et al., 2011; Zheng et al., 2012), was only observed in several recent forest studies (Guédron et al., 2018; Jiskra et al., 2015; Yuan et al., 2020). This is because the relatively small MIF values caused by NVE (less than 0.2‰) and interference of photo-reduction signals derived from litterfall largely limit our ability to identify such processes by a definitive Δ^{199}Hg:Δ^{201}Hg slope. Hg isotope studies have revealed the importance of Hg re-emission caused by microbial Hg reduction, however it is difficult to differentiate the contributions from dark abiotic and microbial reduction to the Hg^0 re-emission from forest floor (Guédron et al., 2018; Kritee et al., 2013).

Given that Hg transport and retention on forest floor are often closely linked to NOM, the stochiometric relations of Hg with carbon (C) and nitrogen (N) have been used as tracers to infer causes and ultimate fates of Hg sequestration in forest ecosystems (Obrist et al., 2009, 2011; Wang et al., 2016b). However, few studies have displayed the relations among isotopes of C, N and Hg. The isotopic fractionation of C and N can be used as a valuable tool for examining the processes of NOM mineralization and transformation (Hobbie and Ouimette, 2009; Natelhoffer and Fry, 1988). These processes are highly involved in the Hg biogeochemical processes, and influence the magnitude and dynamics of Hg and re-emission fluxes from forest floor (Obrist et al., 2018; Wang et al., 2016b). Hence, we hypothesized that interplays among isotopes of C and N would provide a new insight in the sequestration and reduction processes of deposited Hg on forest floor. In this study, we investigated the C, N and Hg isotopic signatures on evergreen broadleaf (EB) forest floor to verify such hypothesis.

2. Methodology

2.1. Study sites

The selected sites are within the Ailaoshan Station for Subtropical Forest Ecosystem Research Studies (ASSFERS, 24°32′N, 101°01′E), which is a pristine EB forest site and has altitudes of 2350 m−2650 m above sea level. Our earlier studies have depicted this site in more detail (Lu et al., 2016; Wang et al., 2016b, 2019c; Yuan et al., 2019a, 2019b, 2020). Briefly, the annual precipitation is 1400 ± 700 mm, average temperature is 13.0 ± 5.0 °C, and relative humidity is 84 ± 5% (Lu et al., 2016; Wang et al., 2016b). The annual average atmospheric Hg^0 concentration is in the range of 1.4−2.0 ng m^{-3}, comparable to the background concentration in the north hemisphere (Zhang et al., 2016a). The dominant tree species are *Castanopsis wattii*, *Lithocarpus xylocarpus*, *Schima noronhae* and *Manglietia insignis*, with canopy heights of 20−30 m and canopy coverage of ≥85%. The forest soil is mainly *Luvisol* (World Reference Base) with a pH of 3.5−4.8 (Yang and Yang, 2011).

2.2. Sample collections and concentration measurements

As shown in Fig. S1 in Supportive Information (SI), seven EB forest sites were selected along the altitude of 2350−2650 m at Mt. Ailao. At each site, five 5 × 5 m subplots were established for sample collection, following our previous protocol at Mt. Ailao (Lu et al., 2016; Wang et al., 2016b). The average thickness of the organic soil horizon (O horizon) was ~15 cm at the elevation of 2450 and 2550 m, and ~10 cm at the elevation of 2350 m and 2650 m. Within the O horizon, the combined Oi (fresh litterfall and twigs) and Oe (partially decomposed litter) was 3−5 cm in thickness in each subplot, with the Oa horizon (well decomposed humus layer) making up the remainder of O horizon. Fresh mature foliage of dominant tree species, Oi, Oe, Oa and 0−10 cm upper mineral soil were collected in each subplot in January 2017.

Vegetation samples were dried in frozen and then grounded by a separate electric grinder. Soil samples were also dried in frozen, grounded in an agate mortar, and sieved by a 200-mesh sieve (74 μm). The Hg concentration in vegetation and soil samples was measured by a DMA80 Hg analyzer. Standard reference materials were measured in every 10 samples, which yielded a recovery of 95−105%. GBW07405 (GSS-5, Hg = 290 ± 40 ng g^{-1}) was utilized as the soil Hg standard, and GBW10020 (GSB-11, Hg = 150 ± 25 ng g^{-1}) and GBW10049 (GSB-27, Hg = 12 ± 3 ng g^{-1}) as the vegetation Hg standards. C and N concentrations were measured by an Elementar Vario Macro Cube analyzer (limit of detection ≤ 10 ppm). Similarly, IVA99994 as the soil C and N standard and AR-2026 as the litter C and N standard were measured in every 10 samples, which yielded recoveries of 97−105%. The detailed concentration data can be found in Tables S1−S2 in SI.

2.3. Isotope measurements

The procedures for Hg isotope measurement were described previously (Wang et al., 2017; 2019a; 2020b). Briefly, all litter and soil samples were processed by a double-stage tube furnace and trapping solutions (anti aqua regia, HNO_3:HCl = 2:1, v/v) for Hg preconcentration, and the Hg solutions were diluted to 1 ng mL^{-1} prior to Hg isotope measurement by the Nu-Plasma II MC-ICP-MS. The acid strength of these diluted solution ranges from 8 to 12%.

The recoveries of preconcentrating were all in the range of 95%–105% for BCR-482 (as the reference standard for vegetation), GSS-4 (590 ± 50 ng g^{-1}, as the reference standard for soil) and samples. $SnCl_2$ (3%) solution was used as the reducing agent for Hg and mixed online with Hg standards or samples to generate Hg^0. Hg concentrations in acid matrices of Hg standard solutions (NIST-3133) and UM-Almadén secondary standard solution were matched to the sample solutions (1 ppb, 10% acid strength in anti-aqua regia solution). Hg-MDF is reported in δ notation using the unit of permil (‰) referenced to the neighboring NIST-3133 solution:

$$\delta^{202}\mathrm{Hg}\left(‰\right) = 1000 \times \left[\left(^{202}\mathrm{Hg}/^{198}\mathrm{Hg}_{\mathrm{sample}}\right)/\left(^{202}\mathrm{Hg}/^{198}\mathrm{Hg}_{\mathrm{NISTSRM3133}}\right) - 1\right] \quad (1)$$

MIF is reported as Δ^{xxx}Hg following the convention suggested by Blum and Bergquist (2007):

$$\Delta^{199}\mathrm{Hg}\ (‰) = \delta^{199}\mathrm{Hg} - 0.2520 \times \delta^{202}\mathrm{Hg} \quad (2)$$

$$\Delta^{200}\mathrm{Hg}\ (‰) = \delta^{200}\mathrm{Hg} - 0.5024 \times \delta^{202}\mathrm{Hg} \quad (3)$$

$$\Delta^{201}\mathrm{Hg}\ (‰) = \delta^{201}\mathrm{Hg} - 0.7520 \times \delta^{202}\mathrm{Hg} \quad (4)$$

UM-Almadén secondary standard solution was analyzed for every 10 samples. To assess if the non-unity recoveries resulting from the double-stage offline combustion-trapping technique induced discernible isotopic bias, we measured BCR 482 as the vegetation reference and GSS-4 as the soil reference at the beginning of sample pre-concentration sessions. Results of UM-Almadén (δ^{202}Hg = −0.54 ± 0.04‰, Δ^{199}Hg = −0.00 ± 0.04‰, Δ^{201}Hg = −0.03 ± 0.02‰, Mean±1SD, Standard deviation, n = 10) and BCR-482 (δ^{202}Hg = −1.67 ± 0.06‰, Δ^{199}Hg = −0.56 ± 0.05‰, Δ^{200}Hg = −0.01 ± 0.03‰, Δ^{201}Hg = −0.58 ± 0.04‰, Mean±1SD, n = 6), and GSS-4 (δ^{202}Hg = −1.72 ± 0.08‰, Δ^{199}Hg = -0.34 ± 0.03‰, Δ^{201}Hg = -0.34 ± 0.03‰, Δ^{200}Hg = −0.00 ± 0.02‰, Mean±1SD, n = 6) are consistent with recommended values (Blum and Bergquist, 2007; Estrade et al., 2010).

δ^{13}C and δ^{15}N ratios in litter and soil samples were analyzed using a Thermo-Fisher MAT 253 (Radke et al., 2012). δ^{13}C and δ^{15}N were calculated as:

$$\delta^{13}\mathrm{C}\left(‰\right) = 1000 \times \left[\left(^{13}\mathrm{C}/^{12}\mathrm{Csample}\right)/\left(^{13}\mathrm{C}/^{12}\mathrm{C}_{\mathrm{P-VDB}}\right) - 1\right] \quad (5)$$

$$\delta^{15}\mathrm{N}\left(‰\right) = 1000 \times \left[\left(^{15}\mathrm{N}/^{14}\mathrm{N}_{\mathrm{sample}}\right)/\left(^{15}\mathrm{N}/^{14}\mathrm{N}_{\mathrm{air}}\right) - 1\right] \quad (6)$$

Duplicated measurements for each sample were performed. Standard samples of IEIA–CH–3 and IEIA-NO3 were measured in every 5 samples. Measured δ^{13}C for IEIA–CH–3 is 24.716 ± 0.035‰ (n = 42, SD, recommended value = -24.724 ± 0.041‰), and δ^{15}N for IEIA-NO3 is 4.7 ± 0.2‰ (n = 42, SD, recommended value = 4.7 ± 0.2‰). The detailed data for all samples can be found in Tables S1 and S2 in SI.

2.4. Calculations of isotopic fractionation on forest floor

To better understand the interplays of isotopic fractionation among Hg, C and N, we defined shifts of isotopic signatures between in soil profile samples and in Oi (i.e., ζ^{202}Hg, ζ^{13}C, ζ^{15}N, Z^{199}Hg and Z^{201}Hg) as:

$$\zeta^{202}\mathrm{Hg}_x = \delta^{202}\mathrm{Hg}_x - \delta^{202}\mathrm{Hg}_{\mathrm{Oi}} \quad (7)$$

$$\zeta^{13}\mathrm{C}_x = \delta^{13}\mathrm{C}_x - \delta^{13}\mathrm{C}_{\mathrm{Oi}} \quad (8)$$

$$\zeta^{15}\mathrm{N}_x = \delta^{15}\mathrm{N}_x - \delta^{15}\mathrm{N}_{\mathrm{oi}} \quad (9)$$

$$Z^{199}\mathrm{Hg}_x = \Delta^{199}\mathrm{Hg}_x - \Delta^{199}\mathrm{Hg}_{\mathrm{Oi}} \quad (10)$$

$$z^{201}\mathrm{Hg}_x = \Delta^{201}\mathrm{Hg}_x - \Delta^{201}\mathrm{Hg}_{\mathrm{Oi}} \quad (11)$$

where x is Oe, Oa, and 0–10 cm mineral soil. The Hg^0 evasion from forest floor to atmosphere can be considered as the product lost reaction in an open system. Hence, we used the Rayleigh Equation to describe the isotopic fractionation:

$$\ln(\delta_R + 1) = \ln(\delta_{R0} + 1) + (\alpha_{P/R} - 1)\ln f \quad (12)$$

where f is the fraction of reactant which remains unutilized (m_R/m_{R0}), and δ_R is the corresponding δ value of reactant remained, and δ_{R0} is the corresponding δ value in the initial condition of reactant, and $\alpha_{P/R}$ is the fractionation factor as $R_{product}/R_{reactant}$. Noting that $\ln(\delta_R+1)$- $\ln(\delta_{R0}+1) \approx \delta_R$- δ_{R0} when δ values ≪ 1 (e.g., δ^{202}Hg ranges 1‰–2‰ ≪ 1 in this study), thus equation of 12 can be simplified as:

$$\zeta = (\alpha_{P/R} - 1)\ln f \quad (13)$$

$$\zeta = \varepsilon_{P/R}\ln f \quad (14)$$

where ζ is isotope shift between δ_R and δ_0 ($\zeta = \delta_R$- δ_{R0}), and $\varepsilon = \alpha_{P/R}$-1. The shift of Hg MIF on forest floor can be calculated using the following equation:

$$Z^{199}\mathrm{Hg} = \Delta^{199}\mathrm{Hg}_R - \Delta^{199}\mathrm{Hg}_{R0} = \delta^{199}\mathrm{Hg}_R - \mathrm{SF}*\delta^{202}\mathrm{Hg}_R - (\delta^{199}\mathrm{Hg}_{R0} - \mathrm{SF}*\delta^{202}\mathrm{Hg}_{R0}) \quad (15)$$

where SF is the mass dependent scaling factor of 0.2520. Combining equations (13) and (15), we obtain:

$$Z^{199}\mathrm{Hg} = (\varepsilon^{199}\mathrm{Hg}_{P/R} - \mathrm{SF}*\varepsilon^{202}\mathrm{Hg}_{P/R})\ln f \quad (16)$$

$$Z^{199}\mathrm{Hg} = E^{199}\mathrm{Hg}*\ln f \quad (17)$$

where E^{199}Hg is the Hg MIF enrichment factor. Given the atmospheric Hg^0 direct deposition, and then oxidation by organic matter

on forest floor as the product accumulated reaction in an open system, the corresponding isotopic relationship can be described as:

$$\delta^{202}Hg_P = \delta^{202}Hg_R\alpha_{P/R} + \varepsilon_{P/R} \quad (18)$$

as $\alpha_{P/R} \approx 1$ for Hg isotopic fractionation, equation (18) can then be simplified as:

$$\delta^{202}Hg_P = \delta^{202}Hg_R + \varepsilon^{202}Hg_{P/R} \quad (19)$$

we also obtain the Hg MIF in product pool during the atmospheric Hg^0 incorporation into forest floor:

$$\Delta^{199}Hg_p = \Delta^{199}Hg_{R0} + E^{199}Hg \quad (20)$$

Using Eq.(12)–(17), we analyzed f (m_R/m_{R0}) versus $\zeta^{202}Hg$ and $Z^{202}Hg$ with the earlier references reported Hg isotope enrichment factors.

2.5. Statistical methods

In this study, One-Way ANOVA was used to analyze statistical differences among the means of Hg, C and N isotopic compositions in each soil horizon. We also used the bivariate Pearson Correlation to produce correlation coefficient among Hg, C, N and their isotopes at 95% or 99% confidence interval by two-tailed T-test. Based on the correlation analysis, we further used conceptual structural equation model (SEM) to construct the interplays among isotope fractionations of Hg, C and N on EB forest floors. SEM was developed from the fully conceptual model using χ^2 tests with maximum likelihood estimation, and more detailed information can be found in our earlier study(Wang et al., 2019b). Briefly, model fitting was performed by using SPSS version 17 and the Amos software version 24. We used p-values (at least > 0.05), χ^2 values and Akaike information criterion (AIC) as the criteria for evaluation of SEM fit. From the SEM path network, the standardized path coefficient (β) represents the direct effect of one variable on another, and the indirect effect is calculated by multiplying each associated β.

3. Results

Fig. 1 shows variations of C, N, Hg and their isotopic compositions in Oi, Oe, Oa and 0–10 cm mineral soil along the elevation of 2350–2650 between the leeward and windward slopes. The C, N, Hg and their isotopic compositions exhibit insignificant difference at the leeward and windward slopes. In addition, the C, N, Hg and their isotopic compositions also do not show a distinct elevation gradient, except the Hg concentrations in Oa and 0–10 mineral soil of 2550 m are higher than values of other elevations.

Fig. 2 displays comparable Hg concentration, Hg/C ratio and isotopic compositions of Hg, C and N between those in mature foliage and Oi (i.e., no significant differences as all $p > 0.05$ by one-Way ANOVA test). There are increasing trends of Hg/C, $\delta^{13}C$, $\delta^{15}N$ and $\delta^{202}Hg$ and decreasing ones of $\Delta^{199}Hg$ and $\Delta^{201}Hg$ signatures in the sequence of foliage, Oi, Oe, Oa and 0–10 cm surface mineral soil (Fig. 2). The Hg MIF signatures in soil profiles, foliage and Oi exhibit distinct negative values (from −0.5 to −0.2‰, Figs. 2 and 3.1), but distinct positive MIF signatures in precipitation (Fig. 3.1). Fig. 3.2 shows a slope of close to ~1.0 for $\Delta^{199}Hg$:$\Delta^{201}Hg$ for all the samples, while slightly more negative $\Delta^{199}Hg$ than $\Delta^{201}Hg$ for surface

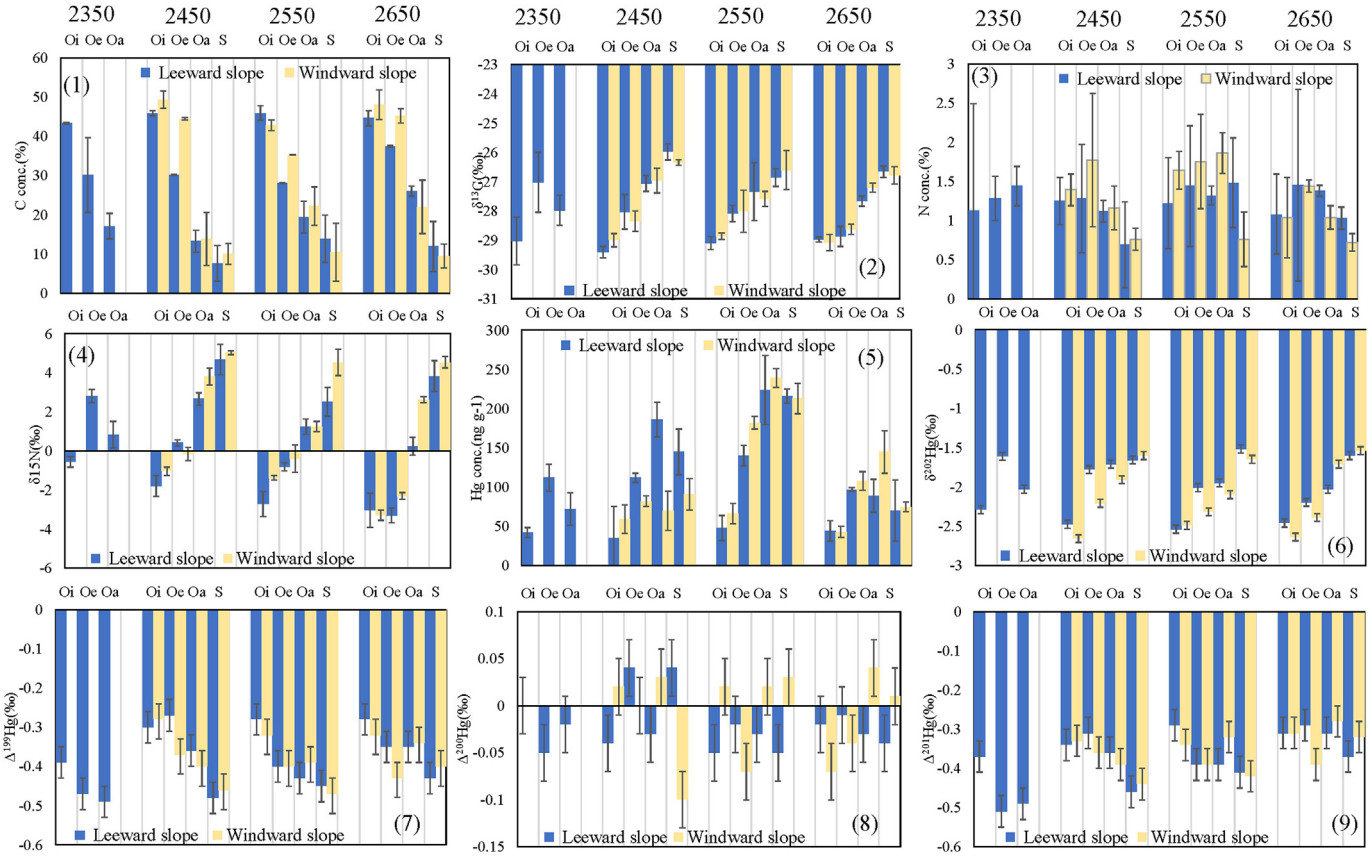

Fig. 1. (1) to (9) Variations of C, N, Hg concentrations (conc.) and their isotopic compositions in Oi, Oe, Oa and 0 to 10 mineral soil (S) along the elevation of 2350–2650 between the leeward and windward slopes at Mt. Ailao. The detailed data can be found in Table S1 in SI.

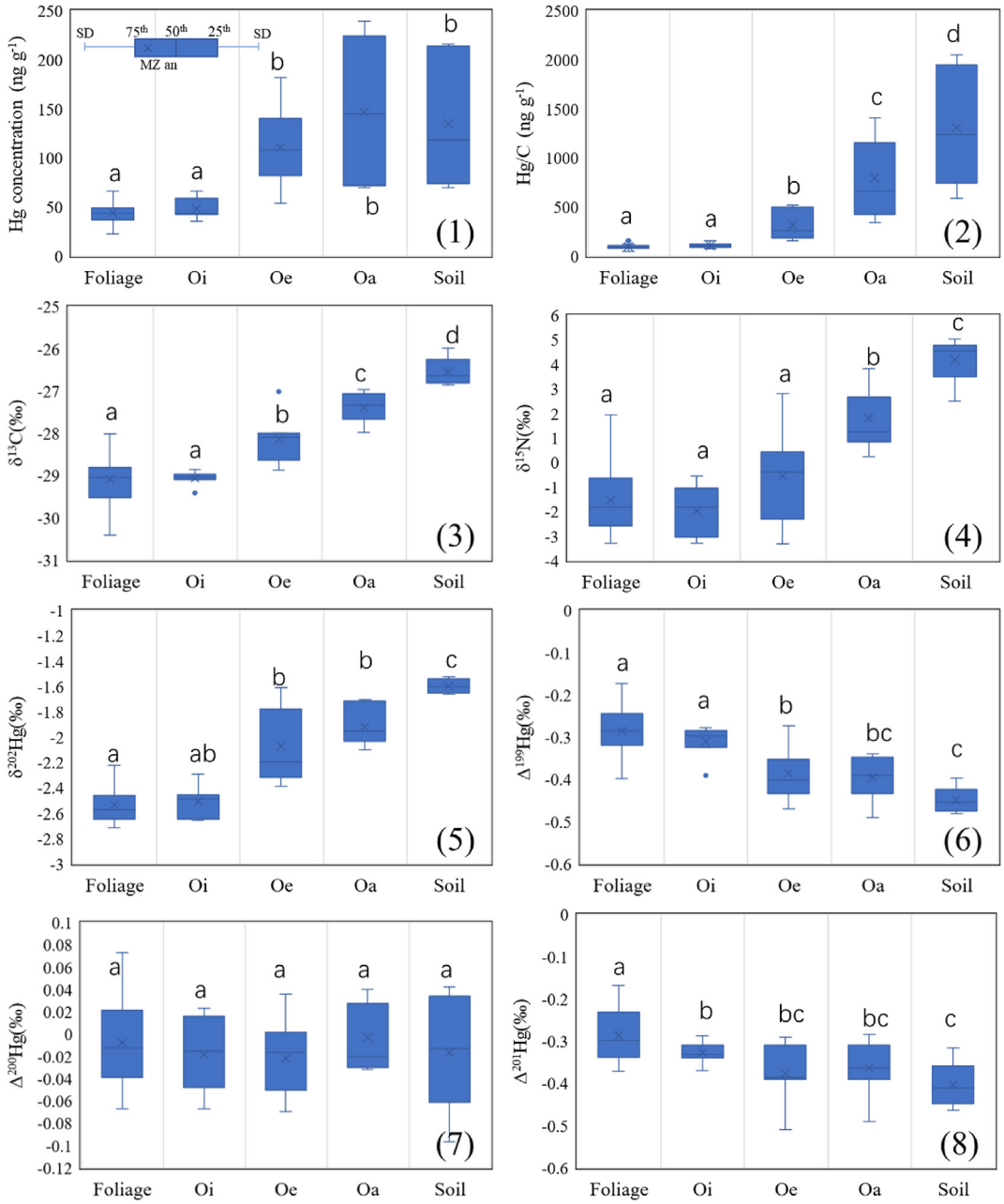

Fig. 2. (1) to (8) Box charts for C, N, Hg and their isotopic signatures in foliage (n = 16), Oi (n = 7 sites), Oe (n = 7 sites), Oa(n = 7 sites), and 0–10 cm mineral soil (n = 7 sites). The One-Way ANOVA tests were performed at 5% significance level, and the letter over the box chart indicates the statistic difference between two terms. The detailed data can be found in Tables S1–S2 in SI.

mineral soil Hg (−0.40 ± 0.05‰ versus −0.38 ± 0.06‰, 1SD, p = 0.094 by Independent Two Samples T-test). It is noteworthy that the relatively small MIF shifts on forest floor (less than −0.2‰) lead to large uncertainties in the slopes of Δ^{199}Hg:Δ^{201}Hg (e.g., r^2 of 0.18 when Δ^{199}Hg scatters with Δ^{201}Hg among Oi, Oe, and Oa samples). Hence, such Δ^{199}Hg:Δ^{201}Hg slope herein cannot be used to identify the occurring of NVE shifts on forest floor.

Significant correlations were identified among Hg, C/N, Hg/C, δ^{13}C, δ^{15}N, δ^{202}Hg, Δ^{199}Hg, and Δ^{201}Hg (Fig. 4 and 5), suggesting the close links of isotopic fractionation among Hg, C and N during litter decomposition and organic matter mineralization on forest floor. Furthermore, ζ^{202}Hg highly correlates with ζ^{15}N and ζ^{13}C, and Z^{199}Hg with Z^{201}Hg and ζ^{13}C in soil profiles (Figs. 4 and 6). The SEM pathway network in Fig. 7 suggests that 83% of the variance of ζ^{202}Hg in soil profiles can be explained by variations of ζ^{13}C, Z^{199}Hg and ζ^{15}N, in which ζ^{15}N has the highest impact (up to 80%). In addition, Z^{201}Hg and ζ^{13}C in soil profiles explain 70% of the variance of Z^{199}Hg. The negative direct effect (−0.54) from ζ^{13}C on Z^{199}Hg in Fig. 7 means the deeper soil organic carbon is with more positive δ^{13}C but more negative Δ^{199}Hg signatures.

4. Discussion

Our earlier studies (Wang et al., 2016b; 2019c) demonstrated that variations in soil Hg were mainly shaped by litterfall depositions and climate changes between the leeward and windward

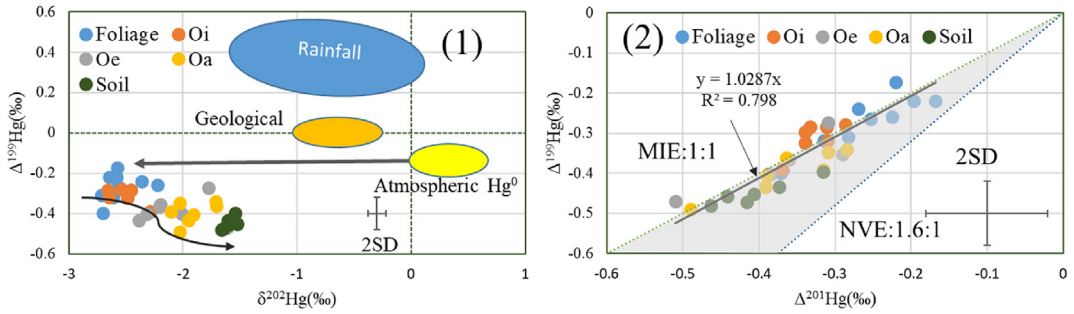

Fig. 3. (1) Mercury isotopic signatures in foliage, Oi, Oe, Oa and 0–10 mineral soil, and in rainfall, geological source and air gas; (2) Δ^{201}Hg versus Δ^{199}Hg in foliage, Oi, Oe, Oa and 0–10 mineral soil. Rainfall Hg, geological Hg and atmospheric Hg^0 isotopic signatures are derived from earlier studies (Blum et al., 2014; Chen et al., 2012; Demers et al., 2013; Fu et al., 2016; Gratz et al., 2010; Sherman et al., 2012; Smith et al., 2008; Yu et al., 2016; Yuan et al., 2015, 2019a).

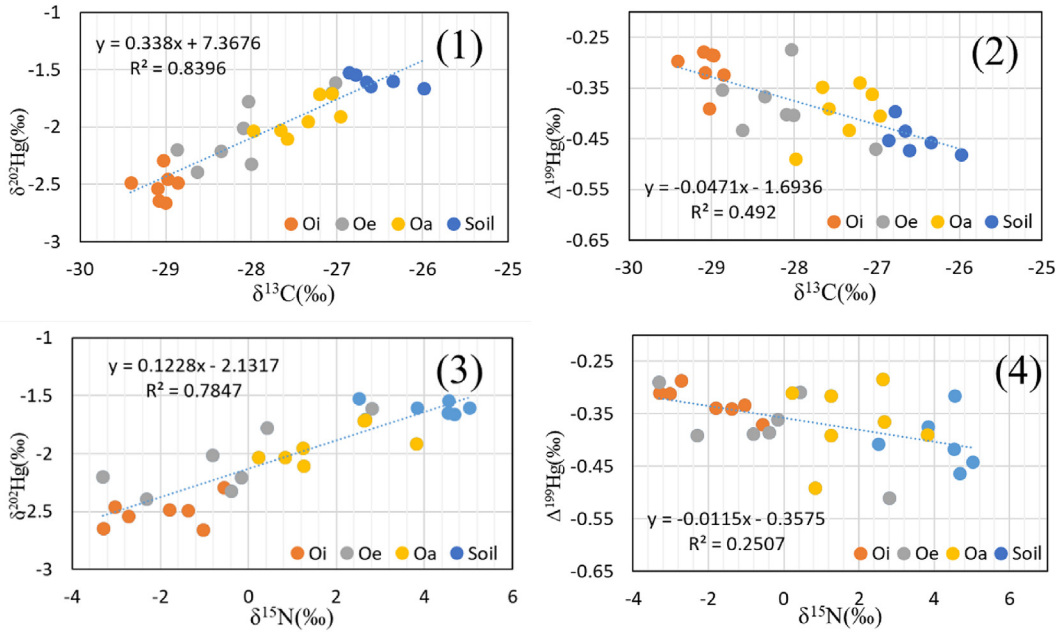

Fig. 4. (1)–(2) δ^{13}C versus δ^{202}Hg and Δ^{199}Hg; (3)–(4) δ^{15}N versus δ^{202}Hg and Δ^{199}Hg along the soil profiles.

sides at Mt. Ailao. Over the elevation of 2350 m, there is little difference for the climate parameters and litterfall Hg deposition fluxes between two sides (Lu et al., 2016; Wang et al., 2016b, 2019c), hence leading to insignificant difference for soil Hg. The Hg isotopic signatures in Figs. 2 and 3.1 further verify this hypothesis that litterfall Hg deposition as the main source for Hg accumulation on forest floor since the negative Hg MIF signatures in soil profiles are much closer to these in foliage and Oi rather than the positive MIF signatures in precipitation. This is also consistent with earlier Hg isotope studies that litterfall Hg is the dominant source for Hg accumulation on forest floor(Jiskra et al., 2015; Wang et al., 2017, 2019b; Zheng et al., 2016). Hence, the present study focuses on Hg sequestration and reduction processes on forest floor through analyzing links among isotopes of C, N and Hg in soil profiles, and does not discuss the elevation gradient among the leeward and windward slope sites.

4.1. Mercury biogeochemical processes revealed by isotopes of Hg, C and N

The process of Hg runoff is not the main cause for Hg isotopic shifts in soil profiles. There are two sources of Hg transported in runoff to downstream from upland headwaters. One is precipitation Hg and the other is the upland surface soil Hg. Several studies have suggested that the Hg runoff mainly as the important Hg post-depositional process on forest floor, and upland soil Hg as the main source (Eklof et al., 2014; Jiskra et al., 2017; Woerndle et al., 2018). Hence, the precipitation Hg isotopic signatures would not significantly shape the Hg isotopic shifts in runoff. In addition, it is well known that NOM plays a governing role in controlling Hg mobility in runoff and stream water. Several studies suggested negligible secondary processes inducing Hg isotopic fractionation since Hg desorbed from soil or decomposing litter as the intact Hg-SOM complexes (Jiskra et al., 2017; Woerndle et al., 2018). Thus, the processes of runoff would not lead to significant Hg isotopic fraction in residual Hg on forest floor.

The geological Hg, derived from weathering of bed rocks, has been shown less negative δ^{202}Hg (−0.6‰ to −1.5‰) than Oi, Oe, Oa and 0–10 cm mineral soil Hg (Fig. 3.1), and no distinct MIF of ^{199}Hg and ^{200}Hg (Blum et al., 2014; Smith et al., 2008). However, the mixing of geological Hg is not the dominant Hg source in Oi, Oe, Oa and 0–10 cm mineral soil in the present study. This conclusion is supported by two evidences. One evidence is that Hg and C concentrations in Oi, Oe, Oa and 0–10 cm mineral soil are one order of

(1) Correlations for soil profile — Sig. < 0.01 — Sig. < 0.05

	δ13C	δ15N	δ202Hg	Δ199Hg	Δ200Hg	Δ201Hg	C	N	Hg	C/N	Hg/C
δ13C		0.96	0.92	-0.78	0.15	-0.61	-0.97	-0.51	0.52	-0.89	0.83
δ15N			0.88	-0.68	0.23	-0.56	-0.93	-0.53	0.41	-0.85	0.75
δ202Hg				-0.65	0.18	-0.44	-0.94	-0.47	0.49	-0.87	0.73
Δ199Hg					0.10	0.82	0.72	0.25	-0.57	0.75	-0.74
Δ200Hg						0.16	-0.16	-0.07	0.10	-0.19	0.19
Δ201Hg							0.52	0.25	-0.38	0.54	-0.63
C								0.51	-0.53	0.91	-0.81
N									0.18	0.14	-0.39
Hg										-0.65	0.76
C/N											-0.75
Hg/C											

(2) Correlations for foliage

	δ13C	δ15N	δ202Hg	Δ199Hg	Δ200Hg	Δ201Hg	C	N	Hg	C/N	Hg/C
δ13C											
δ15N	0.26										
δ202Hg	0.10	0.03									
Δ199Hg	0.06	0.44	-0.05								
Δ200Hg	0.39	0.20	0.18	-0.09							
Δ201Hg	0.39	0.50	0.06	0.74	0.06						
C	0.13	-0.15	-0.09	0.18	-0.09	-0.04					
N	-0.36	0.19	-0.31	0.17	-0.16	-0.06	-0.21				
Hg	-0.12	-0.12	-0.09	-0.19	-0.04	-0.36	-0.13	0.75			
C/N	0.47	-0.24	0.40	-0.02	0.25	0.12	0.40	-0.93	-0.63		
Hg/C	-0.12	-0.07	-0.06	-0.20	-0.02	-0.31	-0.36	0.75	0.97	-0.68	

Fig. 5. (1) to (2) Correlations among C, N, Hg and their isotopic signatures in soil profiles and in foliage.

magnitude greater than those in deep soil and rocks at Mt. Ailao (Hg < 10 ng g^{-1} and C < 1%, respectively) (Wang et al., 2016b), suggesting small proportions of geological Hg mixed in surface soils. The other one is that decreasing Hg MIF signatures were observed with the depth of soil, and such trend is not consistent with the more positive Hg MIF signatures if substantial geological Hg is mixed into the soil. Similarly, earlier studies have suggested the contribution of Hg deposition from the precipitation on Hg accumulation in organic soil profile less than 8% at Mt. Ailao (Wang et al., 2019c; Yuan et al., 2020). Hence, considering that is not a major contributor of Hg sources on forest floor at Mt. Ailao (Fig. 3.1), precipitation Hg input induced Hg isotopic shifts can be ignored.

Photoreduction and volatilization processes also cannot solely explain the Hg isotopic shifts on forest floor. Hg photoreduction with reduced sulfur functional groups can lead to the same direction and magnitude of isotope fractionations in reactants as we observed the positive shift of δ^{202}Hg and negative shift of Δ^{199}Hg on forest floor (Blum et al., 2014). However, forest canopy shading largely diminishes solar radiation on forest floor (Agnan et al., 2016; Obrist et al., 2018), leading to negligible impacts from this reaction on Hg isotopic shifts (Wang et al., 2017). Volatilization of Hg^0 from aqueous solutions with and without DOM would also lead to the reactant enriched with heavier isotopes (Estrade et al., 2009; Zheng et al., 2007). Fig. 8.1 exhibits that such processes induced MDF shift is quite small (nearly 80–90% Hg loss resulting in ~1.0‰). In addition, neither pathways of photo-reduction and volatilization can explain the strong correlations among isotopes of Hg, C and N.

Given that negative Hg^0 flux is often observed on forest floor (Agnan et al., 2016; Zhu et al., 2016), atmospheric Hg^0 direct deposition is likely an additional Hg input on forest floor. The porous nature of litter layers and the high level of organic matter on forest floor can facilitate the sorption of Hg^0 vapor, followed by oxidation by the reduced sulfur functional groups in humic substances (Wang et al., 2016b; Zheng et al., 2016). The Hg isotopic fractionations regarding Hg^0 vapor sorption and dark oxidation by NOM on forest floor are currently with large uncertainties. Under designed laboratory conditions, Zheng et al. (2019) suggests that two reactions are involved in the Hg^0 dark oxidation by NOM. One is the oxidation of Hg^0 to Hg^{2+} caused by thiols with the kinetic isotope effect (KIE), and the other is the equilibrium isotope effect (EIE) between thiol-bound Hg^{2+} and residual Hg^0 vapor (Zheng et al., 2019). Furthermore, Zheng et al. (2019) highlights that total Hg isotopic fractionations are predominantly caused by EIE, leading to enrichment factors for MDF and MIF ($\varepsilon^{202}Hg_{P/R}$ and $E^{199}Hg$) being ranged from 1.10‰ to 1.56‰ and from −0.16‰ to −0.18‰, respectively. The more positive MDF and negative MIF in oxidized Hg are consistent with our observed Hg isotopic shifts on forest floor. However, we suggest Hg^0 vapor dark oxidation by NOM is not the main cause for the observed Hg isotope fractionation on forest floor. This can be attributed to several reasons.

First of all, we used Equations (19) and (20) to verify if Hg^0 vapor dark oxidation by NOM can explain our observations on forest floor. Yu et al. (2016) suggests positive δ^{202}Hg of 0.52 ± 0.30‰ and slightly negative Δ^{199}Hg of −0.18 ± 0.03‰ in atmospheric Hg^0 under forest canopy. Thus, the oxidized Hg as reaction product in NOM should be associated with positive δ^{202}Hg of 1.6‰–2.1‰ and negative Δ^{199}Hg of −0.34‰ to −0.36‰. These Δ^{199}Hg values of oxidized Hg are consistent with our observed MIF in mature foliage and Oi (foliage: −0.29 ± 0.06‰, n = 16; Oi: −0.31 ± 0.04‰, n = 7), but significantly more positive than values in Oe, Oa and 0–10 cm surface mineral soil (all $p < 0.05$, by One-Sample T Test). This indicates that the dark oxidation of Hg^0 vapor by thiols is not the main cause for the Hg MIF shift on forest floor. Secondly, EIE rewrites the KIE caused MDF during Hg^0 oxidation by thiols (Zheng et al., 2019). This process would not lead to C and N isotope fractionations, and thus can hardly explain the observed significant correlations among Hg, C and N isotope shifts on forest floor. Furthermore, worldwide flux measurements depict that the litterfall Hg deposition is always several even tens of times higher than the atmospheric Hg^0 direct deposition flux into forest floor (Agnan et al., 2016; Wang et al., 2016a; Zhang et al., 2016b; Zhu et al., 2016). The air-soil flux measurement at Mt. Ailao shows that Hg evasion during the summertime and deposition during winter, and on the annual level, forest floor serves as a net atmospheric Hg^0 source with emission rate of 6.7 μg m^{-2} yr^{-1} (Yuan et al., 2019b). This indicates the Hg^0 direct deposition flux is not main source for floor Hg. Therefore, we can predict the Hg shift caused by the dark oxidation of Hg^0 vapor would be largely diluted by the litterfall Hg

input. Finally, one field study showed that the residual Hg^0 vapor is with much more positive MDF than the initial atmospheric Hg^0 vapor during air-soil flux exchange (Demers et al., 2013), in contrast to more negative MDF predicted under artificial laboratory conditions (Zheng et al., 2019). Therefore, Hg MDF shift caused by the dark oxidation of Hg^0 vapor alone cannot explain the up to 0.8‰–1.1‰ of $\zeta^{202}Hg$ between in surface soil and Oi.

The microbial mediated NOM decomposition is the main cause for the isotope fractionations of C and N on forest floor (Hobbie and Ouimette, 2009; Natelhoffer and Fry, 1988). Considering the strong correlations among $\zeta^{13}C$, $\zeta^{15}N$ and $\zeta^{202}Hg$, we hypothesize that Hg loss via microbial reduction is the main cause for the distinct Hg MDF shift on forest floor. Earlier studies displayed that microbial reduction would result in typical kinetic MDF with the reactant becoming enriched in heavier isotopes ($\varepsilon^{202}Hg_{P/R}$ ranges −2.0‰ to −1.2‰), but not MIF (Kritee et al., 2007, 2008, 2009). Fig. 8.1 shows the relation between f (m_R/m_{R0}) and $\zeta^{202}Hg$ using reported $\varepsilon^{202}Hg_{P/R}$ of −1.2‰ and −2.0‰ (Kritee et al., 2007, 2008). We found that microbial reduction easily resulted in the distinct shift of MDF in the reactant, and only 25–45% of the reactant loss could lead to $\zeta^{202}Hg$ of ~1‰, a value observed between those in 0–10 cm surface soil and Oi. The 25–45% of the Hg loss during long-term litter and NOM decomposition in EB forest is considered to be reasonable basing on the 500-year Hg isotope fractionation modeling results at Mt. Ailao (Yuan et al., 2020).

Significant correlations were found among $\delta^{13}C$, $\delta^{15}N$ and $\Delta^{199}Hg$ on forest floor (Fig. 4, all $p < 0.05$). Hence, we propose that the dark abiotic reduction by NOM is another cause for Hg isotopic shifts, specifically for MIF shift on forest floor. Bergquist and Blum (2007) reported a dark organically medicated reduction with $\varepsilon^{202}Hg_{P/R}$ of −1.70‰ and $E^{199}Hg_{P/R}$ of 0.03‰. Zheng and Hintelmann (2010b) further suggested that Hg abiotic non-photochemical reduction by bulk DOM (dissolved organic matter) was associated with NVE induced Hg MIF shift ($\Delta^{199}Hg$:$\Delta^{201}Hg$ ~ 1.6), the $\varepsilon^{202}Hg_{P/R}$ of −1.52‰, and $E^{199}Hg_{P/R}$ of 0.38‰. In the present study, we observed about −0.18‰ shift of $\Delta^{199}Hg$ between those in 0–10 cm surface soil and Oi. Figs. 8.1 and 8.2 show that ~35% Hg loss by DOM dark abiotic reduction would result in −0.18‰ shift of $\Delta^{199}Hg$ and 0.65‰ shift of $\delta^{202}Hg$ using the Hg MDF and MIF enrichment factors reported by Zheng and Hintelmann (2010b). In addition, Fig. 6 shows that the correlation coefficient between $\zeta^{13}C$ and $\zeta^{202}Hg$ is much larger than that between $\zeta^{13}C$ and $Z^{199}Hg$. Furthermore, results of SEM verify that the direct effect from $Z^{199}Hg$ on $\zeta^{202}Hg$ is small (0.11, Fig. 7). Therefore, our study indicates the Hg dark abiotic reduction by NOM is the main cause for Hg MIF shifts, but plays a less important role than microbial reduction in shaping the shift of Hg MDF on forest floor.

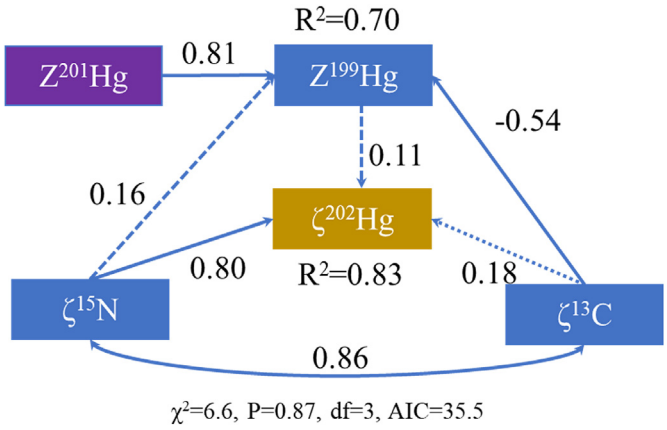

Fig. 7. SEM fitted to soil $\zeta^{202}Hg$ and $\Delta^{199}Hg$ among soil $\zeta^{15}N$ and $\zeta^{13}C$. Numbers adjacent to arrows represent the standardized path coefficients. R^2 indicates the proportion of variance explained. The dot line highlights the path coefficient <0.4.

Yuan et al. (2020) used a multiprocessing isotope fractionation model to estimate the contributions of microbial reduction, photoreduction and dark reduction during post-depositional decomposition of biomass over five centuries at Mt. Ailao. They suggested that microbial reductions play a dominant role in the initial litter decomposition, then dark redox reactions mediated by organic matter become the predominant process (Yuan et al., 2020), consistent with our results herein.

4.2. Relationship between N and Hg biogeochemical cycling in forests

Yuan et al. (2020) has discussed the relationship between Hg, C and their isotopic transitions in soil profile at Mt. Ailao. Briefly, they highlighted the decomposition of soil organic matters releasing the absorbed Hg that is subsequently subject to Hg reduction processes which causing kinetic MDF and odd-MIF in correlation with $\delta^{13}C$ (Yuan et al., 2020). Herein, we would not discuss the correlation among Hg, C and their isotopes. Instead, we observed significant

	$\zeta^{13}C$	$\zeta^{15}N$	$\zeta^{202}Hg$	$Z^{199}Hg$	$Z^{200}Hg$	$Z^{201}Hg$
$\zeta^{13}C$	0.90	0.83	-0.46	0.12	-0.36	
$\zeta^{15}N$	0.90	-0.38	0.24	-0.16		
$\zeta^{202}Hg$	-0.27	0.24	-0.13			
$Z^{199}Hg$	0.30	0.78				
$Z^{200}Hg$	0.36					
$Z^{201}Hg$						

Sig. < 0.01 Sig. < 0.05

Fig. 6. Correlations among $\zeta^{15}N$, $\zeta^{13}C$, $\zeta^{202}Hg$, $Z^{199}Hg$, $Z^{200}Hg$ and $Z^{201}Hg$ in soil profile.

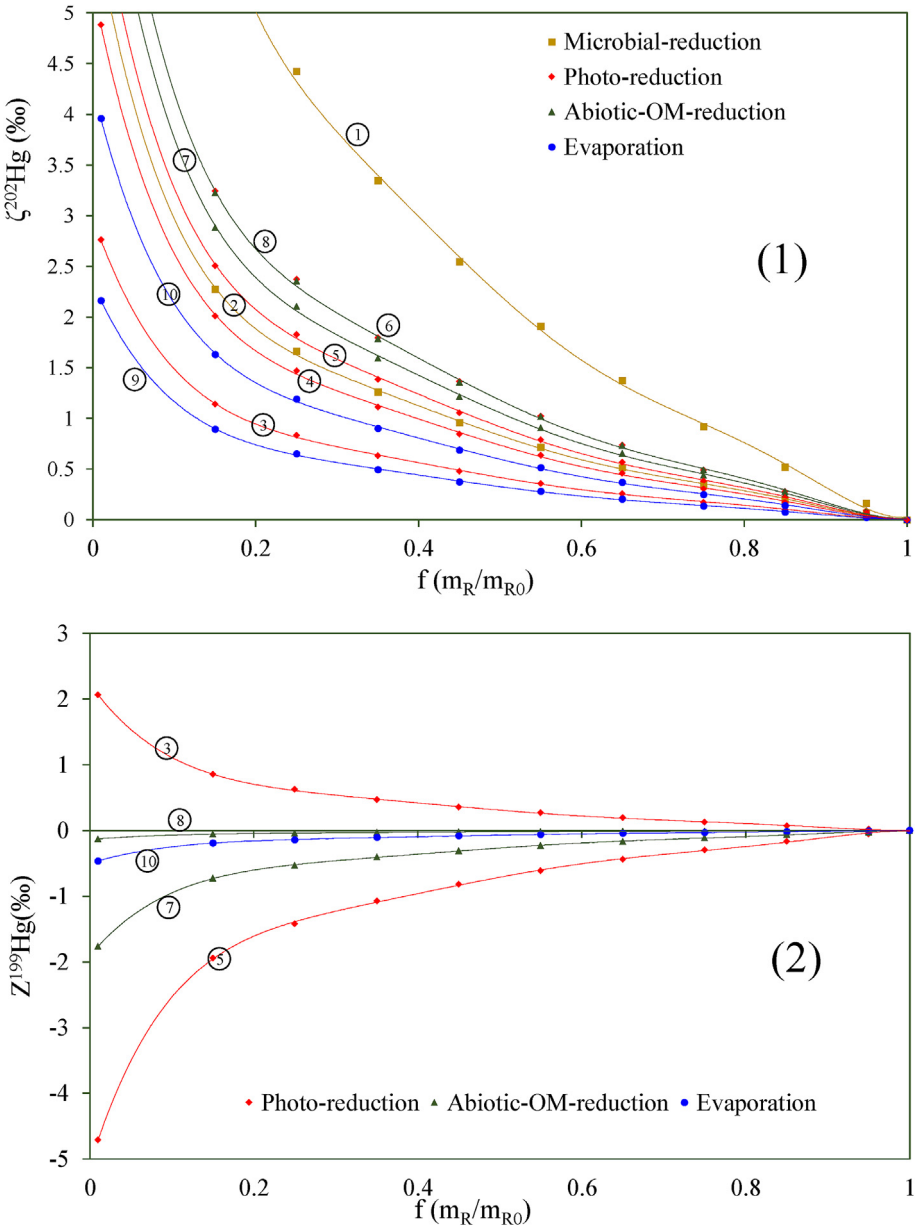

Fig. 8. f (m_R/m_{R0}) versus ζ^{202}Hg and Z^{199}Hg by using earlier references reported Hg isotope enrichment factors. 1 and 2 are from Kritee et al. (2008); Kritee et al. (2007); 3 is from Bergquist and Blum (2007); 4 is from Zheng and Hintelmann (2009); 5 and 6 are from Zheng and Hintelmann (2010a); 7 is from Zheng and Hintelmann (2010b); 8 is from Bergquist and Blum (2007); 9 is from Zheng et al. (2007); 10 is from Estrade et al. (2009).

correlations between Hg and N concentrations both in foliage and soil profiles, consistent with earlier studies (Blackwell and Driscoll, 2015; Obrist et al., 2012). Furthermore, Fig. 6 exhibit that ζ^{202}Hg in soil profiles is strongly correlated to ζ^{15}N, which explains 80% of the variability of ζ^{202}Hg. These phenomena suggest distinct links between N and Hg biogeochemical cycling in the EB forests.

Blackwell and Driscoll (2015) suggested that the strong correlation between Hg and N in foliage can be attributed to both N and Hg derived from long-range transport of industrial atmospheric pollution. However, we hardly observe a strong correlation between atmospheric Hg^0 and N concentrations at Mt. Ailao because of complicated impacts from different sources, and dilutions during long-range transports (Wang et al., 2015; Zhang et al., 2016a). In fact, high energy resolution X-ray absorption near-edge structure (HR-XANES) spectroscopy exhibits Hg mainly as the species of Hg $[(SR)_2 + (N/O)_{1-2}]$ stored in leaf interior (Manceau et al., 2018), providing new evidence for explaining the strong link between N and Hg in foliage.

Litter decomposition represents the primary source of nutrients or energy both for plants and microbes. This is particularly true for the availability of soil N, which has no notable geological input in forest ecosystem, and the supply of N has been generally considered as the essential and growth-limiting factors (Elser et al., 2007). Thus, the N microbial mineralization on forest floor would increase the N/O and reduce organic S functional groups associated with protein production on forest floor (Demers et al., 2007; Wang et al., 2016b). XANES studies have well documented that soft Group B metals such as Hg in NOM is associated with reduced organic S and N/O functional groups (Manceau et al., 2015, 2018; Skyllberg et al., 2006). Hence, Hg accumulation on forest floor is distinctly related

to the N/O functional group formation during the microbial mineralization, consistent with the strong correlation between Hg and N concentrations in soil profiles observed in this study.

Theoretically, N concentration can be used as an index to determine net N release and immobilization on forest floor because N release occurs when there is enough N supply for microbial decomposers and external N immobilization from environment typically occurs when N is at low levels. Global-scale long term litter decomposition data identified that, regardless of climate, edaphic and biota conditions, initial foliage N concentration is the dominant factor to drive net N release from decomposing leaf litter (Parton et al., 2007). Parton et al. (2007) demonstrated that continuous N release occurs during litter decomposition when foliage N > 1.0% because decomposers meet their N requirements directly from the litter. In this study, the N concentration in foliage ranges from 1.0% to 1.6% with the average value of 1.3 ± 0.3%, thereby suggesting a net N release during litter decomposition. The N release leads to heavier N isotope on forest floor, consistent with our observed increasing $\delta^{15}N$ with the depth of soil profile. The N release by microbial decomposition of litter and NOM is also associated with the mineralization of C and functional groups, such as N/O and reduced organic S in NOM (Homann and Cole, 1990; Houle et al., 2001; Schroth et al., 2007), thus simultaneously releasing absorbed Hg from NOM. The absorbed Hg in following is subject to the Hg^0 re-emission via microbial and small organic matter molecules induced reduction (Briggs and Gustin, 2013). Therefore, we attribute the cause of the strong correlations between $\delta^{202}Hg$ and $\delta^{15}N$, and between $\zeta^{202}Hg$ and $\zeta^{15}N$ in soil profiles to the complicated microbial processes induced Hg^0 and N release. In addition, the strong correlation between $\delta^{15}N$ and $\delta^{13}C$ ($r = 0.96$, $p < 0.01$) is suggestive of C loss during litter and NOM decomposition on forest floor, and also explains the strong correlation between $\delta^{202}Hg$ and $\delta^{15}C$ in soil profiles because of the collinearity of C and N.

The changes of N deposition may influence Hg cycling in forest ecosystems. The dramatically growth of industrialization and agricultural intensification have resulted in significant increase of anthropogenic emissions for active N compounds and associated enhanced N deposition in terrestrial ecosystems, e.g. with global N deposition at the level of 60 Tg N yr^{-1} in 1990s and expected to reach 125 Tg N yr^{-1} by 2050 (Galloway et al., 2004). Enhanced N deposition has been profoundly changing the nutrient cycling in forest ecosystems, e.g. up to 175 Pg C taken up by terrestrial ecosystems as a result of the increased N deposition since the pre-industrial period (Bala et al., 2013; Galloway et al., 2004). Given an average of ~50 ng g^{-1} C of Hg/C ratio in terrestrial ecosystems (Jiskra et al., 2018; Obrist et al., 2011), we estimate that Hg deposition has been increased by about ~8750 Mg due to enhanced N deposition during the same period. In addition, increased N deposition in forests has negative effects on soil microbial abundance and composition, leading to a reduced microbial respiration and an enhanced carbon sequestration on forest floor (Maaroufi et al., 2015; Zhang et al., 2018). The enhanced carbon sequestration by additional N deposition likely influences litter Hg sequestration on forest floor. However, few studies have reported to date the relation between Hg re-emission and N deposition in forest ecosystems except one study in peatland which exhibited that the enhanced N deposition had no significant effect on air-soil Hg fluxes (Fritsche et al., 2014). The implications of the strong link between N and Hg cycling in forest ecosystems requires further studies and the relationships between Hg, N and C in terrestrial ecosystems need to be verified by additional research globally.

5. Conclusions

In this study, we have identified the microbial Hg reduction as the main cause for the Hg MDF shift and dark abiotic NOM reduction for the Hg MIF shift on forest floor by analyzing Hg, C, N and their isotope data. We also have found that higher N in foliage can lead to greater Hg concentration, and N release and immobility on forest floor is closely linked to the microbial reduction induced Hg^0 re-emission. We recommend further studies focus on the close relationships between Hg and N biogeochemical processes in terrestrial ecosystems to verify the hypothesis that the elevated atmospheric N loading likely influence Hg cycling in global forest ecosystems.

Declaration of competing interest

The authors declare that they have no known competing financial interests or personal relationships that could have appeared to influence the work reported in this paper.

Acknowledgments

This work was funded by National Natural Science Foundation of China (41703135), Yunnan Natural Science Foundation (2019FB064), and Fundamental Research Funds for the Central Universities (SWU019037), and National Natural Science Foundation of China (41977272). The dataset of concentration and isotopic compositions can be found in Supportive Information.

Appendix A. Supplementary data

Supplementary data to this article can be found online at https://doi.org/10.1016/j.envpol.2020.115867.

References

Agnan, Y., Le Dantec, T., Moore, C.W., Edwards, G.C., Obrist, D., 2016. New constraints on terrestrial surface atmosphere fluxes of gaseous elemental mercury using a global database. Environ. Sci. Technol. 50, 507–524.
Bala, G., Devaraju, N., Chaturvedi, R.K., Caldeira, K., Nemani, R., 2013. Nitrogen deposition: how important is it for global terrestrial carbon uptake? Biogeosciences 10, 7147–7160.
Bergquist, B.A., Blum, J.D., 2007. Mass-dependent and -independent fractionation of Hg isotopes by photoreduction in aquatic systems. Science 318, 417–420.
Blackwell, B.D., Driscoll, C.T., 2015. Using foliar and forest floor mercury concentrations to assess spatial patterns of mercury deposition. Environ. Pollut. 202, 126–134.
Blum, J.D., Bergquist, B.A., 2007. Reporting of variations in the natural isotopic composition of mercury. Anal. Bioanal. Chem. 388, 353–359.
Blum, J.D., Sherman, L.S., Johnson, M.W., 2014. Mercury isotopes in earth and environmental sciences. Annu. Rev. Earth Planet Sci. 42, 249–269.
Briggs, C., Gustin, M.S., 2013. Building upon the conceptual model for soil mercury flux: evidence of a link between moisture evaporation and Hg evasion. Water, Air, Soil Pollut. 224, 1744.
Chen, J.B., Hintelmann, H., Feng, X.B., Dimock, B., 2012. Unusual fractionation of both odd and even mercury isotopes in precipitation from Peterborough, ON, Canada. Geochem. Cosmochim. Acta 90, 33–46.
Demers, J.D., Blum, J.D., Zak, D.R., 2013. Mercury isotopes in a forested ecosystem: implications for air-surface exchange dynamics and the global mercury cycle. Global Biogeochem. Cycles 27, 222–238.
Demers, J.D., Driscoll, C.T., Fahey, T.J., Yavitt, J.B., 2007. Mercury cycling in litter and soil in different forest types in the Adirondack region, New York, USA. Ecol. Appl. 17, 1341–1351.
Eklof, K., Schelker, J., Sorensen, R., Meili, M., Laudon, H., von Bromssen, C., Bishop, K., 2014. Impact of forestry on total and methyl-mercury in surface waters: distinguishing effects of logging and site preparation. Environ. Sci. Technol. 48, 4690–4698.
Elser, J.J., Bracken, M.E.S., Cleland, E.E., Gruner, D.S., Harpole, W.S., Hillebrand, H., Ngai, J.T., Seabloom, E.W., Shurin, J.B., Smith, J.E., 2007. Global analysis of nitrogen and phosphorus limitation of primary producers in freshwater, marine and terrestrial ecosystems. Ecol. Lett. 10, 1135–1142.

Estrade, N., Carignan, J., Sonke, J.E., Donard, O.F.X., 2009. Mercury isotope fractionation during liquid-vapor evaporation experiments. Geochem. Cosmochim. Acta 73, 2693–2711.
Estrade, N., Carignan, J., Sonke, J.E., Donard, O.F.X., 2010. Measuring Hg isotopes in bio-geo-environmental reference materials. Geostand. Geoanal. Res. 34, 79–93.
Fritsche, J., Osterwader, S., Nilsson, M.B., Sagerfors, J., Akerblom, S., Bishop, K., Alewell, C., 2014. Evasion of elemental mercury from a boreal peat land suppressed by long-term sulfate addition. Environ. Sci. Technol. Lett. 1, 421–425.
Fu, X., Marusczak, N., Wang, X., Gheusi, F., Sonke, J.E., 2016. Isotopic composition of gaseous elemental mercury in the free troposphere of the pic du Midi observatory, France. Environ. Sci. Technol. 50, 5641–5650.
Galloway, J.N., Dentener, F.J., Capone, D.G., Boyer, E.W., Howarth, R.W., Seitzinger, S.P., Asner, G.P., Cleveland, C.C., Green, P.A., Holland, E.A., Karl, D.M., Michaels, A.F., Porter, J.H., Townsend, A.R., Vöosmarty, C.J., 2004. Nitrogen cycles: past, present, and future. Biogeochemistry 70, 153–226.
Gratz, L.E., Keeler, G.J., Blum, J.D., Sherman, L.S., 2010. Isotopic composition and fractionation of mercury in great lakes precipitation and ambient air. Environ. Sci. Technol. 44, 7764–7770.
Grigal, D.F., 2002. Inputs and outputs of mercury from terrestrial watersheds: a review. Environ. Rev. 10, 1–39.
Gu, B., Bian, Y., Miller, C.L., Dong, W., Jiang, X., Liang, L., 2011. Mercury reduction and complexation by natural organic matter in anoxic environments. Proc. Natl. Acad. Sci. U. S. A. 108, 1479–1483.
Guédron, S., Amouroux, D., Tessier, E., Grimaldi, C., Barre, J., Berail, S., Perrot, V., Grimaldi, M., 2018. Mercury isotopic fractionation during pedogenesis in a tropical forest soil catena (French guiana): deciphering the impact of historical gold mining. Environ. Sci. Technol. 52, 11573–11582.
Gustin, M.S., Lindberg, S.E., Weisberg, P.J., 2008. An update on the natural sources and sinks of atmospheric mercury. Appl. Geochem. 23, 482–493.
Hobbie, E.A., Ouimette, A.P., 2009. Controls of nitrogen isotope patterns in soil profiles. Biogeochemistry 95, 355–371.
Homann, P.S., Cole, D.W., 1990. Sulfur dynamics in decomposing forest litter: relationship to initial concentration, ambient sulfate and nitrogen. Soil Biol. Biochem. 22, 621–628.
Houle, D., Carignan, R., Ouimet, R., 2001. Soil organic sulfur dynamics in a coniferous forest. Biogeochemistry 53, 105–124.
Jiskra, M., Sonke, J.E., Obrist, D., Bieser, J., Ebinghaus, R., Myhre, C.L., Pfaffhuber, K.A., Wangberg, I., Kyllonen, K., Worthy, D., Martin, L.G., Labuschagne, C., Mkololo, T., Ramonet, M., Magand, O., Dommergue, A., 2018. A vegetation control on seasonal variations in global atmospheric mercury concentrations. Nat. Geosci. 11, 244–250.
Jiskra, M., Wiederhold, J.G., Skyllberg, U., Kronberg, R.-M., Hajdas, I., Kretzschmar, R., 2015. Mercury deposition and Re-emission pathways in boreal forest soils investigated with Hg isotope signatures. Environ. Sci. Technol. 49, 7188–7196.
Jiskra, M., Wiederhold, J.G., Skyllberg, U., Kronberg, R.-M., Kretzschmar, R., 2017. Source tracing of natural organic matter bound mercury in boreal forest runoff with mercury stable isotopes. Environ Sci-Proc Imp 19, 1235–1248.
Kritee, K., Barkay, T., Blum, J.D., 2009. Mass dependent stable isotope fractionation of mercury during mer mediated microbial degradation of monomethylmercury. Geochem. Cosmochim. Acta 73, 1285–1296.
Kritee, K., Blum, J.D., Barkay, T., 2008. Mercury stable isotope fractionation during reduction of Hg(II) by different microbial pathways. Environ. Sci. Technol. 42, 9171–9177.
Kritee, K., Blum, J.D., Johnson, M.W., Bergquist, B.A., Barkay, T., 2007. Mercury stable isotope fractionation during reduction of Hg(II) to Hg(0) by mercury resistant microorganisms. Environ. Sci. Technol. 41, 1889–1895.
Kritee, K., Blum, J.D., Reinfelder, J.R., Barkay, T., 2013. Microbial stable isotope fractionation of mercury: a synthesis of present understanding and future directions. Chem. Geol. 336, 13–25.
Lindberg, S., Bullock, R., Ebinghaus, R., Engstrom, D., Feng, X.B., Fitzgerald, W., Pirrone, N., Prestbo, E., Seigneur, C., 2007. A synthesis of progress and uncertainties in attributing the sources of mercury in deposition. Ambio 36, 19–32.
Lu, Z.Y., Wang, X., Zhang, Y.P., Zhang, Y.J., Luo, K., Sha, L.Q., 2016. High mercury accumulation in two subtropical evergreen forests in South China and potential determinants. J. Environ. Manag. 183, 488–496.
Maaroufi, N.I., Nordin, A., Hasselquist, N.J., Bach, L.H., Palmqvist, K., Gundale, M.J., 2015. Anthropogenic nitrogen deposition enhances carbon sequestration in boreal soils. Global Change Biol. 21, 3169–3180.
Manceau, A., Lemouchi, C., Enescu, M., Gaillot, A.C., Lanson, M., Magnin, V., Glatzel, P., Poulin, B.A., Ryan, J.N., Aiken, G.R., Gautier-Luneau, I., Nagy, K.L., 2015. Formation of mercury sulfide from Hg(II)-Thiolate complexes in natural organic matter. Environ. Sci. Technol. 49, 9787–9796.
Manceau, A., Wang, J.X., Rovezzi, M., Glatzel, P., Feng, X.B., 2018. Biogenesis of mercury-sulfur nanoparticles in plant leaves from atmospheric gaseous mercury. Environ. Sci. Technol. 52, 3935–3948.
Natelhoffer, K.J., Fry, B., 1988. Controls on natural nitrogen-15 and carbon-13 abundances in forest soil organic matter. Soil Sci. Soc. Am. J. 52, 1633–1640.
Obrist, D., Johnson, D.W., Edmonds, R.L., 2012. Effects of vegetation type on mercury concentrations and pools in two adjacent coniferous and deciduous forests. J. Plant Nutr. Soil Sci. 175, 68–77.
Obrist, D., Johnson, D.W., Lindberg, S.E., 2009. Mercury concentrations and pools in four Sierra Nevada forest sites, and relationships to organic carbon and nitrogen. Biogeosciences 6, 765–777.
Obrist, D., Johnson, D.W., Lindberg, S.E., Luo, Y., Hararuk, O., Bracho, R., Battles, J.J., Dail, D.B., Edmonds, R.L., Monson, R.K., Ollinger, S.V., Pallardy, S.G., Pregitzer, K.S., Todd, D.E., 2011. Mercury distribution across 14 US forests. Part I: spatial patterns of concentrations in biomass, litter, and soils. Environ. Sci. Technol. 45, 3974–3981.
Obrist, D., Kirk, J.L., Zhang, L., Sunderland, E.M., Jiskra, M., Selin, N.E., 2018. A review of global environmental mercury processes in response to human and natural perturbations: changes of emissions, climate, and land use. Ambio 47, 116–140.
Parton, W., Silver, W.L., Burke, I.C., Grassens, L., Harmon, M.E., Currie, W.S., King, J.Y., Adair, E.C., Brandt, L.A., Hart, S.C., Fasth, B., 2007. Global-scale similarities in nitrogen release patterns during long-term decomposition. Science 315, 361–364.
Pokharel, A.K., Obrist, D., 2011. Fate of mercury in tree litter during decomposition. Biogeosciences 8, 2507–2521.
Radke, J., Deerberg, M., Hilkert, A., Schlüter, H.J., Schwieters, J., 2012. High resolution double-focusing isotope ratio mass spectrometry. Egu General Assembly 14, 12549.
Schroth, A.W., Bostick, B.C., Graham, M., Kaste, J.M., Mitchell, M.J., Friedland, A.J., 2007. Sulfur species behavior in soil organic matter during decomposition. J Geophys Res-Biogeo 112, 1–10.
Sherman, L.S., Blum, J.D., Keeler, G.J., Demers, J.D., Dvonch, J.T., 2012. Investigation of local mercury deposition from a coal-fired power plant using mercury isotopes. Environ. Sci. Technol. 46, 382–390.
Skyllberg, U., Bloom, P.R., Qian, J., Lin, C.-M., Bleam, W.F., 2006. Complexation of mercury(II) in soil organic Matter: EXAFS evidence for linear two-coordination with reduced sulfur groups. Environ. Sci. Technol. 40, 4174–4180.
Smith, C.N., Kesler, S.E., Blum, J.D., Rytuba, J.J., 2008. Isotope geochemistry of mercury in source rocks, mineral deposits and spring deposits of the California Coast Ranges, USA. Earth Planet Sci. Lett. 269, 398–406.
Sonke, J.E., 2011. A global model of mass independent mercury stable isotope fractionation. Geochem. Cosmochim. Acta 75, 4577–4590.
UN-Environment, 2019. Global Mercury Assessment 2018. UN-environment Programme. Chemicals and Health Branch, Geneva, Switzerland.
Wang, X., Bao, Z., Lin, C.-J., Yuan, W., Feng, X., 2016a. Assessment of global mercury deposition through litterfall. Environ. Sci. Technol. 50, 8548–8557.
Wang, X., Lin, C.-J., Lu, Z., Zhang, H., Zhang, Y., Feng, X., 2016b. Enhanced accumulation and storage of mercury on subtropical evergreen forest floor: implications on mercury budget in global forest ecosystems. J Geophys Res-Biogeo 121, 2096–2109.
Wang, X., Luo, J., Yin, R., Yuan, W., Lin, C.-J., Sommar, J., Feng, X., Wang, H., Lin, C., 2017. Using mercury isotopes to understand mercury accumulation in the montane forest floor of the eastern Tibetan plateau. Environ. Sci. Technol. 51, 801–809.
Wang, X., Luo, J., Yuan, W., Lin, C.J., Wang, F., Liu, C., Wang, G., Feng, X., 2020a. Global warming accelerates uptake of atmospheric mercury in regions experiencing glacier retreat. Proc. Natl. Acad. Sci. U. S. A. 117, 2049–2055.
Wang, X., Yuan, W., Feng, X., Wang, D., Luo, J., 2019a. Moss facilitating mercury, lead and cadmium enhanced accumulation in organic soils over glacial erratic at Mt. Gongga, China. Environ. Pollut. 254, 112974.
Wang, X., Yuan, W., Lin, C.J., Luo, J., Wang, F., Feng, X., Fu, X., Liu, C., 2020b. Underestimated sink of atmospheric mercury in a deglaciated forest chronosequence. Environ. Sci. Technol. 54, 8083–8093.
Wang, X., Yuan, W., Lin, C.J., Zhang, L.M., Zhang, H., Feng, X.B., 2019b. Climate and vegetation as primary drivers for global mercury storage in surface soil. Environ. Sci. Technol. 53, 10665–10675.
Wang, X., Yuan, W., Lu, Z.Y., Lin, C.J., Yin, R.S., Li, F., Feng, X.B., 2019c. Effects of precipitation on mercury accumulation on subtropical montane forest floor: implications on climate forcing. J Geophys Res-Biogeo 124, 959–972.
Wang, X., Zhang, H., Lin, C.J., Fu, X.W., Zhang, Y.P., Feng, X.B., 2015. Transboundary transport and deposition of Hg emission from springtime biomass burning in the Indo-China Peninsula. J. Geophys. Res. Atmos. 120, 9758–9771.
Whitehead, D., 2011. Forests as carbon sinks—benefits and consequences. Tree Physiol. 31, 893–902.
Woerndle, G.E., Tsz-Ki Tsui, M., Sebestyen, S.D., Blum, J.D., Nie, X., Kolka, R.K., 2018. New insights on ecosystem mercury cycling revealed by stable isotopes of mercury in water flowing from a headwater peatland catchment. Environ. Sci. Technol. 52, 1854–1861.
Yang, Z., Yang, X.D., 2011. Characteristics of floor litter and soil arthropod community in different types of subtropical forest in Ailao Mountain of Yunnan,-Southwest China. Chin. J. Appl. Ecol. 22, 3011–3020.
Yu, B., Fu, X., Yin, R., Zhang, H., Wang, X., Lin, C.-J., Wu, C., Zhang, Y., He, N., Fu, P., 2016. Isotopic composition of atmospheric mercury in China: new evidence for sources and transformation processes in air and in vegetation. Environ. Sci. Technol. 50, 9262–9269.
Yuan, S., Zhang, Y., Chen, J., Kang, S., Zhang, J., Feng, X., Cai, H., Wang, Z., Wang, Z., Huang, Q., 2015. Large variation of mercury isotope composition during a single precipitation event at Lhasa City, Tibetan Plateau, China. In: Millot, R., Negrel, P. (Eds.), 11th Applied Isotope Geochemistry Conference Aig-11, pp. 282–286.
Yuan, W., Sommar, J., Lin, C.-J., Wang, X., Li, K., Liu, Y., Zhang, H., Lu, Z., Wu, C., Feng, X., 2019a. Stable isotope evidence shows Re-emission of elemental mercury vapor occurring after reductive loss from foliage. Environ. Sci. Technol. 53, 651–660.
Yuan, W., Wang, X., Lin, C.-J., Sommar, J., Lu, Z., Feng, X., 2019b. Process factors driving dynamic exchange of elemental mercury vapor over soil in broadleaf forest ecosystems. Atmos. Environ. 219, 117047.
Yuan, W., Wang, X., Lin, C.J., Wu, C., Zhang, L., Wang, B., Sommar, J., Lu, Z., Feng, X.,

2020. Stable mercury isotope transition during postdepositional decomposition of biomass in a forest ecosystem over five centuries. Environ. Sci. Technol. 14, 8739–8749.
Zhang, H., Fu, X.W., Lin, C.J., Shang, L.H., Zhang, Y.P., Feng, X.B., Lin, C., 2016a. Monsoon-facilitated characteristics and transport of atmospheric mercury at a high-altitude background site in southwestern China. Atmos. Chem. Phys. 16, 13131–13148.
Zhang, H., Yin, R.S., Feng, X.B., Sommar, J., Anderson, C.W.N., Sapkota, A., Fu, X.W., Larssen, T., 2013. Atmospheric mercury inputs in montane soils increase with elevation: evidence from mercury isotope signatures. Sci Rep-Uk 3, 3322.
Zhang, L.M., Lyman, S., Mao, H.T., Lin, C.J., Gay, D.A., Wang, S.X., Gustin, M.S., Feng, X.B., Wania, F., 2017. A synthesis of research needs for improving the understanding of atmospheric mercury cycling. Atmos. Chem. Phys. 17, 9133–9144.
Zhang, L.M., Wu, Z.Y., Cheng, I., Wright, L.P., Olson, M.L., Gay, D.A., Risch, M.R., Brooks, S., Castro, M.S., Conley, G.D., Edgerton, E.S., Holsen, T.M., Luke, W., Tordon, R., Weiss-Penzias, P., 2016b. The estimated six-year mercury dry deposition across north America. Environ. Sci. Technol. 50, 12864–12873.
Zhang, T.a., Chen, H.Y.H., Ruan, H., 2018. Global negative effects of nitrogen deposition on soil microbes. ISME J. 12, 1817–1825.
Zheng, W., Demers, J.D., Lu, X., Bergquist, B.A., Anbar, A.D., Blum, J.D., Gu, B., 2019. Mercury stable isotope fractionation during abiotic dark oxidation in the presence of thiols and natural organic matter. Environ. Sci. Technol. 53, 1853–1862.
Zheng, W., Foucher, D., Hintelmann, H., 2007. Mercury isotope fractionation during volatilization of Hg(0) from solution into the gas phase. J. Anal. Atomic Spectrom. 22, 1097–1104.
Zheng, W., Hintelmann, H., 2009. Mercury isotope fractionation during photoreduction in natural water is controlled by its Hg/DOC ratio. Geochem. Cosmochim. Acta 73, 6704–6715.
Zheng, W., Hintelmann, H., 2010a. Isotope fractionation of mercury during its photochemical reduction by low-molecular-weight organic compounds. J. Phys. Chem. 114, 4246–4253.
Zheng, W., Hintelmann, H., 2010b. Nuclear field shift effect in isotope fractionation of mercury during abiotic reduction in the absence of light. J. Phys. Chem. 114, 4238–4245.
Zheng, W., Liang, L., Gu, B., 2012. Mercury reduction and oxidation by reduced natural organic matter in anoxic environments. Environ. Sci. Technol. 46, 292–299.
Zheng, W., Obrist, D., Weis, D., Bergquist, B.A., 2016. Mercury isotope compositions across North American forests. Global Biogeochem. Cycles 30, 1475–1492.
Zhu, W., Lin, C.J., Wang, X., Sommar, J., Fu, X., Feng, X., 2016. Global observations and modeling of atmosphere–surface exchange of elemental mercury: a critical review. Atmos. Chem. Phys. 16, 4451–4480.